Regenerative Therapy 14 (2020) 252–261

Contents lists available at ScienceDirect

Regenerative Therapy

journal homepage: http://www.elsevier.com/locate/reth

Original Article

Development of a non-alcoholic steatohepatitis model with rapid accumulation of fibrosis, and its treatment using mesenchymal stem cells and their small extracellular vesicles

Takayuki Watanabe [a], Atsunori Tsuchiya [a, *], Suguru Takeuchi [a], Shunsuke Nojiri [a], Tomoaki Yoshida [a], Masahiro Ogawa [a], Michiko Itoh [b], Masaaki Takamura [a], Takayoshi Suganami [c], Yoshihiro Ogawa [d], Shuji Terai [a, **]

[a] Division of Gastroenterology and Hepatology, Graduate School of Medical and Dental Sciences, Niigata University, 1-757, Asahimachi-dori, Chuo-ku, Niigata, 951-8510, Japan
[b] Kanagawa Institute of Industrial Science and Technology, 3-25-13, Tonomachi, Kawasaki-ku, Kawasaki, Japan
[c] Department of Molecular Medicine and Metabolism, Research Institute of Environmental Medicine, Nagoya University, Furu-cho, Chikusa-ku, Nagoya, 464-8601, Japan
[d] Department of Medicine and Bioregulatory Science, Graduate School of Medical Sciences, 3-1-1, Maidashi, Higashi-ku, Fukuoka, 812-8582, Japan

ARTICLE INFO

Article history:
Received 16 December 2019
Received in revised form
29 February 2020
Accepted 18 March 2020

Keywords:
Non-alcoholic steatohepatitis
Cirrhosis
Mesenchymal stem cells
Small extracellular vesicles

ABSTRACT

Introduction: Currently, there are no approved drugs for treating non-alcoholic steatohepatitis (NASH); however, mesenchymal stem cells (MSCs) and their small extracellular vesicles (sEVs), which possess immunomodulatory activities, are potential candidates. This study aimed to develop a mouse model of NASH with rapid accumulation of fibrosis using the pre-established melanocortin type-4 receptor knockout (*Mc4r*-KO) NASH mouse model and lipopolysaccharide (LPS), and to evaluate the therapeutic effect of MSCs and their sEVs.

Methods: *Mc4r*-KO mice (8 weeks old, male) were fed a western diet (WD) for 8 weeks. Next, the mice were intraperitoneally injected with lipopolysaccharide (LPS) twice a week for 4 weeks while continuing the WD. To confirm the therapeutic effect of MSCs and sEVs, human adipose tissue-derived MSCs or their sEVs were administered 12 weeks after initiation of the WD, and serum testing, quantitative analysis of fibrosis, and quantitative reverse transcription-polymerase chain reaction qRT-PCR were performed.

Results: By providing a WD combined with LPS treatment, we successfully developed a NASH model with rapid accumulation of fibrosis. Both human MSCs and their sEVs decreased serum alanine transaminase levels and inflammatory markers based on qRT-PCR. Histological analysis showed that MSC or sEV treatment did not affect fat accumulation. However, an improvement in fibrosis in the groups treated with MSCs and their sEVs was observed. Furthermore, after administering MSCs and sEVs, there was a significant increase in anti-inflammatory macrophages in the liver.

Conclusion: We successfully developed a NASH model with rapid accumulation of fibrosis and confirmed the anti-inflammatory and anti-fibrotic effects of MSCs and their sEVs, which may be options for future therapy.

Abbreviations: ALT, alanine transaminase; MSC, mesenchymal stem cell; sEV, small extracellular vesicle; HCC, hepatocellular carcinoma; hCLS, hepatic crown-like structure; MC4R, melanocortin-4 receptor-deficient; MCD, methionine-choline-deficient diet; ND, normal diet; NAFLD, non-alcoholic fatty liver disease; NASH, non-alcoholic steatohepatitis; T-bil, total bilirubin; T-cho, total cholesterol; WD, Western diet.

* Corresponding author. Niigata University, 1-757 Asahimachi-dor, Chuo-ku, Niigata, 951-8510, Japan. Fax: +81-25-227-0776.
** Corresponding author.
E-mail addresses: dogood.10.12@gmail.com (T. Watanabe), atsunori@med.niigata-u.ac.jp (A. Tsuchiya), sugu01@med.niigata-u.ac.jp (S. Takeuchi), snojiri@med.niigata-u.ac.jp (S. Nojiri), tomomot.1105@gmail.com (T. Yoshida), mogawamasa@med.niigata-u.ac.jp (M. Ogawa), mito.mem@tmd.ac.jp (M. Itoh), atmc@med.niigata-u.ac.jp (M. Takamura), suganami@riem.nagoya-u.ac.jp (T. Suganami), yogawa@intmed3.med.kyushu-u.ac.jp (Y. Ogawa), terais@med.niigata-u.ac.jp (S. Terai).

Peer review under responsibility of the Japanese Society for Regenerative Medicine.

https://doi.org/10.1016/j.reth.2020.03.012

1. Introduction

Currently, the incidence of non-alcoholic fatty liver disease (NAFLD), which is often associated with metabolic syndrome and type 2 diabetes mellitus, is increasing worldwide. Non-alcoholic steatohepatitis (NASH), which is a part of NAFLD, is characterized by inflammation and fibrosis of the liver, and can eventually lead to hepatocellular carcinoma; thus, NASH is one of the most important causes of chronic liver diseases, including cirrhosis [1]. Several factors such as consumption of a high-fat diet (HFD), genetic factors such as Patatin-like phospholipase domain-containing protein 3 *(PNPLA3)*-associated NAFLD, oxidative stress, production of excessive cytokines and adipokines, overexpression of toll-like receptors (TLRs), and inflammation caused by gut-derived factors such as lipopolysaccharide (LPS) are responsible for the development of NASH [2]. According to the multiple-parallel hit hypothesis, these complex pathological conditions act as multiple insults on a predisposed individual, leading to the development of NAFLD.

An appropriate mouse model that reflects the complex pathological conditions of NASH is required for studying this disease. Melanocortin-4 receptor-deficient (*Mc4r*-KO) mice fed an HFD or Western diet (WD) have been reported as a NASH model with a phenotype similar to that of human NASH. MC4R is expressed in the hypothalamic nuclei, where it regulates food intake and bodyweight; hence, *Mc4r*-KO mice cannot control their appetite and exhibit symptoms similar to those of human NASH, such as obesity, insulin resistance, and liver steatosis. When HFD was started 8 weeks after birth, steatohepatitis with fibrosis was observed 28 weeks after birth, and hepatocellular carcinoma occurred approximately 1 year after birth. Thus, the effect of drugs used for treating steatosis, fibrosis, and carcinogenesis can be evaluated using this mouse model [3–8]; however, the time required for manifestation of the NASH disease conditions is long, which is a drawback of using this model.

In addition, the dearth of drugs that can reduce inflammation or fibrosis is another bottleneck in NASH research. Currently, drugs approved for NASH treatment in the clinical setting are absent, and exercise therapy and diet therapy are considered fundamental for obtaining favorable outcomes. Mesenchymal stem cells (MSCs) and their sEVs are being studied in the treatment of various diseases, including cirrhosis and acute liver diseases [9–11]. MSCs, which possess multipotent differentiation ability and low antigenicity, can self-renew and differentiate into adipocytes, cartilage, and bone; currently, their immunosuppressive and modulatory activities are attracting attention. MSCs are often termed “medical signaling cells” or “conducting cells” and can be cultured from not only bone marrow but also medical waste such as adipose tissue and umbilical cord tissues [12]. MSCs, which secrete cytokines, chemokines, growth factors, and sEVs, have been shown to improve fibrosis and promote liver regeneration in a liver cirrhosis model. Our previous study elucidated that MSCs can change the polarity of macrophages toward an anti-inflammatory phenotype and indirectly contribute to fibrosis regression in a cirrhosis mouse model. MSC-derived sEVs can transport cargo such as proteins, lipids, and microRNAs (miRNAs) to reduce acute liver injury and improve liver fibrosis in cases of chronic liver injury. sEVs have also attracted attention as one of the mechanisms of tissue repair by MSCs [10,11,13–16].

In the present study, based on the multiple-parallel hit hypothesis, we used the pre-established *Mc4r*-KO NASH mouse model and lipopolysaccharide (LPS), which can induce inflammation, to establish NASH faster than in the previously established model. We evaluated the therapeutic effect of MSCs and their sEVs using this new mouse model.

2. Materials and methods

2.1. Mouse

Mc4r-KO mice with a C57BL/6J background were provided by Joel K. Elmquist (University of Texas Southern Medical Center, Dallas, TX, USA) [17]. Four randomly selected mice were housed in individual cages with a 12 h day/night cycle and were allowed free access to food and water. All animal experiments were conducted in compliance with the regulations and approval of the Institutional Animal Care Committee of the Niigata University. The NASH model mice were developed using Western diet (WD; Research Diets, Inc., New Brunswick, NJ, USA)-fed-*Mc4r*-KO mice from 8 weeks of age. The mice were fed a normal diet until 8 weeks (ND; CE-2; CLEA Japan, Inc. Tokyo, Japan).

2.2. LPS

LPS (Sigma–Aldrich, Tokyo, Japan; LPS from *Escherichia coli* O111:B4; catalog number L2630) was dissolved in phosphate-buffered saline (PBS) (0.1 mg/ml), and 0.3 mg/kg LPS was injected intraperitoneally twice a week.

2.3. MSCs

Human adipose tissue-derived mesenchymal stem cells (AD-MSCs; passage 2) were obtained from PromoCell (Heidelberg, Germany; catalog number C-12977) and expanded until passage 4 using MSC growth medium DXF (catalog number C-28010) in the presence of 5% CO_2 at 37 °C. Mice were administered 1×10^6 cells.

2.4. sEVs

Conditioned medium isolated from MSC culture was collected and centrifuged at 2000×*g* for 10 min to remove the cells and cell debris. The supernatant was then filtered using Stericup® Quick Release (Millipore Corporation, Billerica, MA, USA) and centrifuged using an SW41Ti rotor (Beckman Coulter, Brea, CA, USA) and Optima XL-100 K ultracentrifuge (Beckman Coulter) at 125,000×*g* for 70 min at 4 °C. The sEVs were washed in PBS and recentrifuged at the same speed before resuspending in 100 μl PBS. sEV size was confirmed using a Nanosight (mean size = ~100 nm) and electron microscopy. The total protein was quantified using QubitR following the manufacturer's instructions. Mice were administered 1.0 μg, 2.5 μg, or 5.0 μg of sEVs.

2.5. Immunohistochemistry

For staining of the liver tissue, 10% formalin-fixed tissue was cut into 4-μm-thick sections. The paraffin sections were deparaffinized, rehydrated, and stained with hematoxylin and eosin (H & E) and Sirius Red for histological examination following the manufacturer's standard protocols. Immunohistochemistry for F4/80 (Abcam, Cambridge, UK; ab111101; rabbit monoclonal to F4/80, dilution 1/200), TLR4 (Abcam; ab13867; rabbit monoclonal to TLR4, dilution 1/100), and alpha smooth muscle actin (αSMA; Abcam; ab124964; rabbit monoclonal to αSMA, dilution 1/50) was performed as follows. The dewaxed tissues were subjected to antigen retrieval using a microwave in 10 mM sodium citrate buffer, pH 6.0, for 20 min. Endogenous peroxidase activity was blocked by treatment with 3% H_2O_2 in PBS for 10 min at room temperature, followed by avidin-biotin blocking. Each antibody was applied overnight in antibody diluent reagent solution (Thermo Fisher Scientific, Waltham, MA, USA). The secondary antibody reaction was performed using the

Vecstain ABC kit (Vector Laboratories, Burlingame, CA, USA). The sections were colored by reaction with DAB TRIS tablets (Muto Pure Chemicals, Tokyo, Japan). The number of F4/80-positive cells was counted in at least 20 fields at 400 × magnification.

2.6. Analysis of fibrosis

Hepatic collagen content was measured using the Sirius Red-stained tissue and ImageJ software (version 1.6.0 20, National Institutes of Health, Bethesda, MD, USA).

2.7. Serum test

Blood samples were taken from the heart of the mice four weeks after cell or sEV injection. Serum alanine aminotransferase (ALT), alkaline phosphatase (ALP), total bilirubin (T-bil), total cholesterol (T-cho), albumin (ALB), glucose, glycoalbumin (GA), triglyceride (TG), and free fatty acid (FFA) levels were determined by the Oriental Yeast Co., Ltd (OYC, headquarter Tokyo, Japan).

2.8. Quantitative reverse transcription-polymerase chain reaction (qRT-PCR)

Total RNA was extracted from the liver using the RNeasy kit (Qiagen, Hilden, Germany) and QuantiTect reverse transcription kit (Qiagen) according to the manufacturer's protocol. The RNA concentration was determined using a NanoDrop spectrophotometer (Thermo Fisher Scientific, Schwerte, Germany). Primers were purchased from Qiagen. qRT-PCR was performed using a Step One Plus Real-Time PCR System (Applied Biosystems, Foster City, CA, USA). *Gapdh* was used as the internal control, and the ΔΔCt method was used to analyze the fold change in relative gene expression with respect to the control.

2.9. Flow cytometric analysis

The liver was perfused with PBS and dissected finely. The dissected tissues were then pressed through 200-gauge stainless steel mesh and suspended in Eagle's minimal essential medium (MEM) supplemented with 5 mM HEPES (Nissui Pharmaceutical Co., Tokyo, Japan) and 2% heat-inactivated newborn calf serum. After washing, the cells were fractionated via centrifugation in 15 ml 35% Percoll solution (Pharmacia Fine Chemicals, Piscataway, NJ, USA) for 15 min at 2000 rpm. The pellet was resuspended in an erythrocyte-lysing solution (ACK Lysing Buffer; Thermo Fisher Scientific). The single-cell suspensions obtained were stained with a mixture of appropriate anti-mouse antibodies and analyzed using FACSCalibur (Becton Dickinson; BD; Franklin Lakes, NJ, USA).

2.10. Statistical analyses

Statistical analyses were performed using the GraphPad Prism6 software (GraphPad Software Inc., La Jolla, CA, USA). Data are presented as means ± SD. Differences between groups were analyzed using one-way analysis of variance (ANOVA). $P < 0.05$ was considered statistically significant.

3. Results

3.1. Inflammation in LPS-treated Mc4r-KO mice was stronger than in control mice

Initially, we aimed to establish a mouse model with rapid NASH development using the *Mc4r*-KO mouse. Toward this, we divided mice into three groups. For the control mice, WD was started from 8 weeks after birth and continued for 12 weeks. PBS was injected during the last 4 weeks twice a week (12W control model). To determine the effect of LPS, WD was started from 8 weeks after birth and continued for 12 weeks; LPS was injected twice a week during the last 4 weeks (12W LPS model). For comparison with the 12W model, WD was started from 8 weeks after birth and continued for 20 weeks (20W model) (Fig. 1a). Bodyweight (Fig. 2a) and the liver-to-body weight ratio (Fig. 2b) were highest in the 20W model, and the 12W LPS ($p < 0.05$) and 20W models ($p < 0.05$) tended to show higher ALT levels (Fig. 2c) compared to the 12W control model. T-cho levels did not differ significantly between the three groups; however, serum T-bil levels in the 20W model were significantly higher ($p < 0.05$) than those in the 12W control model (Fig. 2c), serum ALB levels in the 12W LPS model were significantly lower ($p < 0.01$) than those in the 12W control model, and serum TG levels in the 12W control model were significantly higher than those in the 12W LPS model ($p < 0.05$) and 20W model ($p < 0.05$) (Fig. 2c). qRT-PCR using liver tissue revealed that the mRNA levels of *Il6*, *Tnfa*, and *Timp1* in the 12W LPS model (*Il6*; $p < 0.05$, *Tnfa*; $p < 0.05$, *Timp1*; $p < 0.05$) and 20W model (*Il6*; $p < 0.05$, *Tnfa*; $p < 0.05$, *Timp1*; $p < 0.01$) were significantly higher than those in the 12W control model, and that the mRNA levels did not differ significantly between the 12W LPS and 20W models (Fig. 2d). These results suggested that inflammation was stronger in the 12W LPS model than in the 12W control model and was more similar to that in the 20W model.

3.2. LPS-treated Mc4r-KO mice showed accelerated formation of crown-like structures (CLS) and earlier formation of fibrosis than control mice

We performed H & E staining, Sirius Red staining, and F4/80 immunohistochemistry to assess changes in hepatic damage and fibrosis in all groups. First, we evaluated fibrosis using Sirius Red staining (Fig. 3a). Quantitative analysis of the Sirius Red-stained area showed that fibrosis was significantly higher in the 12W LPS model (10.4 ± 2.9%; $p < 0.01$) and 20W model (11.6 ± 4.8%; $p < 0.01$) than in the 12W control model (2.6 ± 0.9%), and that there was no significant difference between the 12W LPS model and the 20W model (Fig. 3b). Next, immunohistochemistry for F4/80 revealed that the number of CLS in the 12W LPS model (26.1 ± 2.0 cells/field; $p < 0.01$) and 20W model (28.2 ± 0.7 cells/field; $p < 0.01$) was significantly higher than that in the 12W control model (15.1 ± 1.5 cells/field), and that there was no significant difference in CLS number between the 12W LPS and 20W models (Fig. 3c). In the F4/80-positive area, we observed relatively strong TLR4 and αSMA expression, suggesting that macrophage activation and fibrogenesis are correlated. Taken together, these results suggested that the 12W LPS and 20W models were similar in terms of the number of CLS and extent of fibrosis, indicating that the 12W LPS model showed rapid development of NASH.

3.3. Adipose tissue-derived MSCs and their sEVs attenuated inflammation and reduced fibrosis in the rapid NASH fibrosis model

Next, based on the 12W LPS model, we evaluated the therapeutic effect of AD-MSCs and AD-MSC-derived sEVs, which were injected once 4 weeks prior to analysis. Three different doses of sEVs were evaluated, namely, 1.0 μg, 2.5 μg, and 5.0 μg (Fig. 1b). The bodyweight and liver-to-body weight ratio revealed no significant difference between the control (PBS) group, MSC injection group, and sEV injection groups (1.0 μg, 2.5 μg, and 5.0 μg) (Fig. 4a and b). The serum levels of ALT, T-cho, T-bil, ALB, glucose, GA, TG, and FFA showed that while there was no significant difference in

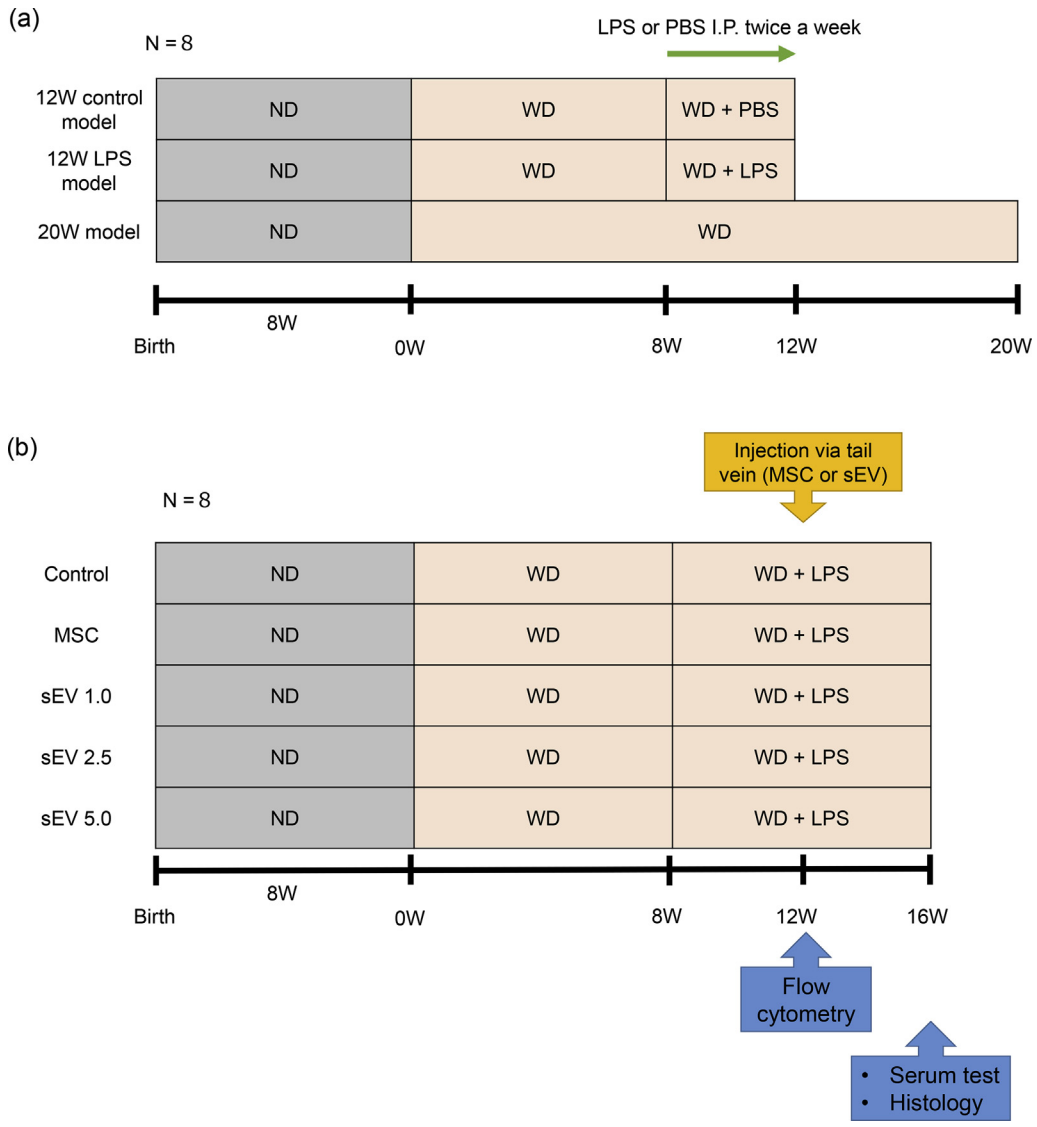

Fig. 1. Experimental protocol. (a) *Mc4r*-KO mice were fed a WD from 8 weeks of age and followed up for an additional 12 weeks; they were fed PBS (12W control model; n = 8) or LPS (12W LPS model; n = 8) for the last 4 weeks. The 20W control model (n = 8), which was fed a WD from 8 weeks of age and followed up for an additional 20 weeks, was set up as a positive control for the 12W LPS model. (b) *Mc4r*-KO mice were fed a WD from 8 weeks of age and followed up for 16 weeks. LPS was administered 8 weeks from the start of the WD and continued until 16 weeks. Twelve weeks from the start of WD, PBS (n = 8), MSCs (n = 8), or sEVs (1.0, 2.5, and 5.0 μg/mouse; sEV1.0, sEV2.5, and sEV5.0, respectively; n = 8 per group) were administered via the tail vein. Cytometry analysis was performed 24 h after MSC or sEV therapy, and serum testing, quantitative analysis of fibrosis, and real-time PCR using liver tissues were performed 4 weeks after MSC or sEV injection.

T-bil, ALB, glucose, GA, TG, and FFA levels between the groups, serum ALT levels tended to decrease after both MSC and sEV injection. In particular, the effect was dose-dependent, and compared to the control, injection of 5.0 μg sEVs significantly decreased the serum levels of ALT ($p < 0.05$) (Fig. 4c). Furthermore, the extent of fibrosis observed using Sirius Red staining (Fig. 5a and c) and the number of CLS (Fig. 5b and d) decreased after MSC and sEV treatment, which was indicative of the therapeutic effect of AD-MSCs and sEVs in all groups. The therapeutic effect was dose-dependent; the AD-MSC group (Sirius Red; $p < 0.01$, CLS; $p < 0.01$) and the 2.5 μg (Sirius Red; $p < 0.05$, CLS; $p < 0.05$) and 5.0 μg sEV (Sirius Red; $p < 0.01$, CLS; $p < 0.01$) groups showed significantly improved fibrosis and a decrease in the number of CLS compared to the control, suggesting that the therapeutic effect of sEVs was similar to that of MSCs when a sufficient amount of sEVs were used.

3.4. Number of anti-inflammatory macrophages in the liver increased after MSC or sEV injection

We and others have previously reported that MSCs can affect the polarity of macrophages [10]. Hence, we determined the number of anti-inflammatory macrophages (CD11b + F4/80 + Ly6c^{low}) among CD11b + F4/80+ macrophages 24 h after injection of AD-MSCs or 5 μg sEVs. Both AD-MSCs and sEVs significantly increased the number of CD11b + F4/80 + Ly6c^{low} anti-inflammatory macrophages in the liver (Fig. 6a). Furthermore, we analyzed the levels of the *Mmp2, 8, 12,* and 13 mRNAs using qRT-PCR. *Mmp12* and 13 mRNA levels in the sEV injection group were significantly higher ($p < 0.05$) than those in the control groups (Fig. 6b). These results indicated that MSC or MSC-derived sEV injection increased the frequency of anti-inflammatory macrophages in the liver, which might contribute to the maintenance of hepatic homeostasis.

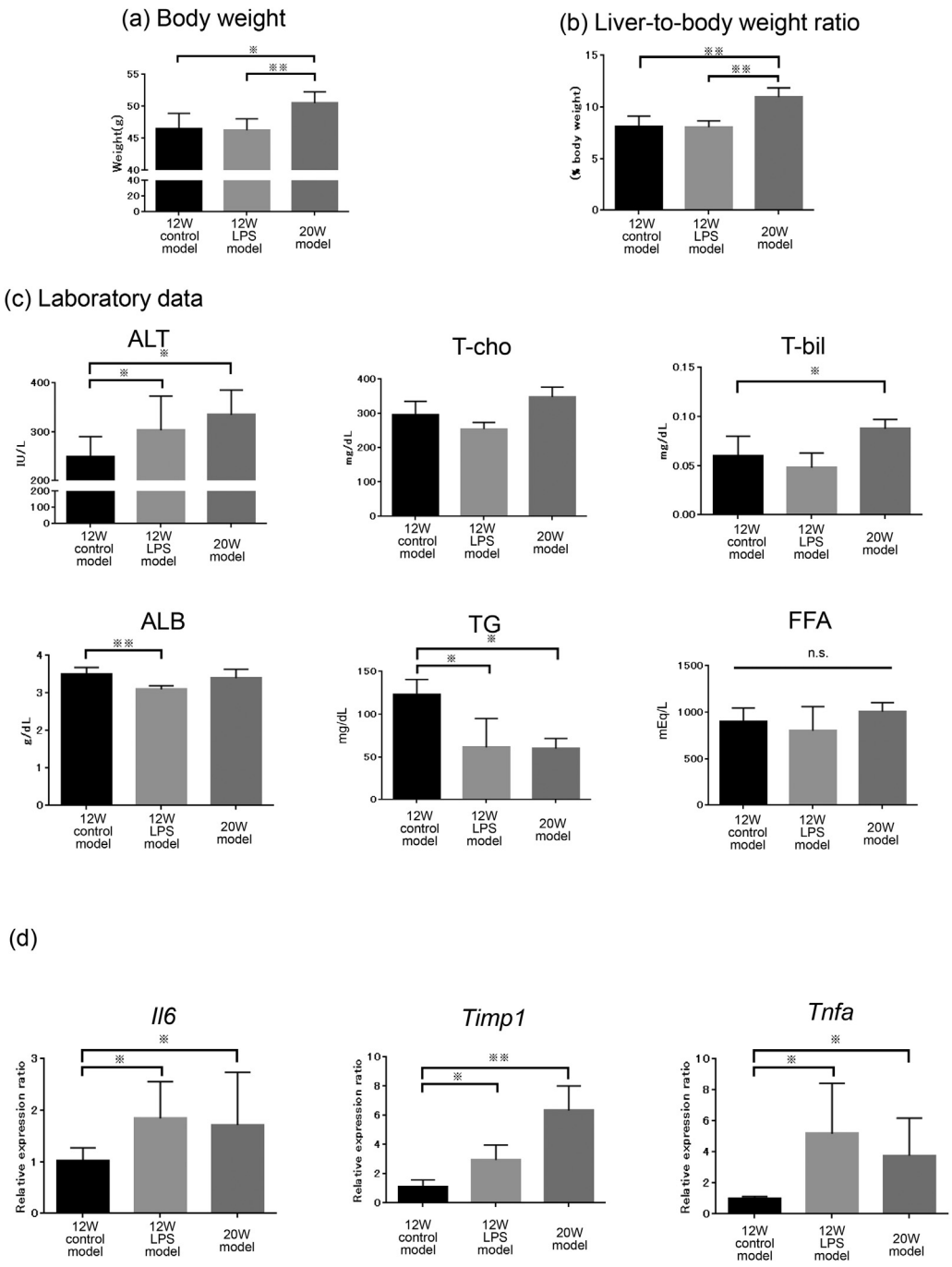

Fig. 2. Analysis of the effect of LPS. (a) Bodyweight, (b) liver-to-body weight ratio, and (c) serum laboratory data of ALT, T-cho, TG, T-bil, ALB, and FFA were determined in the 12W control model, 12W LPS model, and 20W control model (n = 8 for each group) (※p < 0.05, ※※p < 0.01, one-way ANOVA, Bonferroni test). (d) Changes in the mRNA expression of *Il-6*, *Timp1*, *and Tnfa* in each group (n = 8 for each group) were analyzed using qRT-PCR (※p < 0.05, ※※ p < 0.01, one-way ANOVA, Bonferroni test). ALT, alanine transaminase; T-cho, total cholesterol; TG, triglycerides; T-bil, total bilirubin; ALB, albumin; FFA, free fatty acid.

4. Discussion

In this study, we developed a new NASH model using *Mc4r*-KO mice fed a WD and LPS. The transaminase levels, the number of CLS, and fibrosis increased after LPS administration, resulting in a relatively rapid development of NASH. Furthermore, we confirmed that both AD-MSCs and their sEVs possess anti-inflammatory and anti-fibrotic effects using the rapid NASH model.

Despite the availability of several experimental NASH mouse models, replication of the natural course of human NASH development in these models is challenging. Traditionally, methionine/choline-deficient (MCD) mice are used for studying NASH; however, although these mice develop fatty liver, their body weight decreases rapidly, and they do not show insulin resistance [18]. WD is widely used to induce pathological NASH. It induces obesity and insulin resistance; however, the induction of severe steatosis and advanced fibrosis cannot be achieved even after prolonged WD administration. Several groups have attempted to establish NASH models that can mimic human NASH. Tsuchida et al. treated C57BL/6 mice on a WD with carbon tetrachloride (CCl_4) to establish rapid progressive NASH [18]. Liebig et al. injected C57BL/6 mice with 200 μg streptozotocin (STZ) (which destroys β cells in the islet of

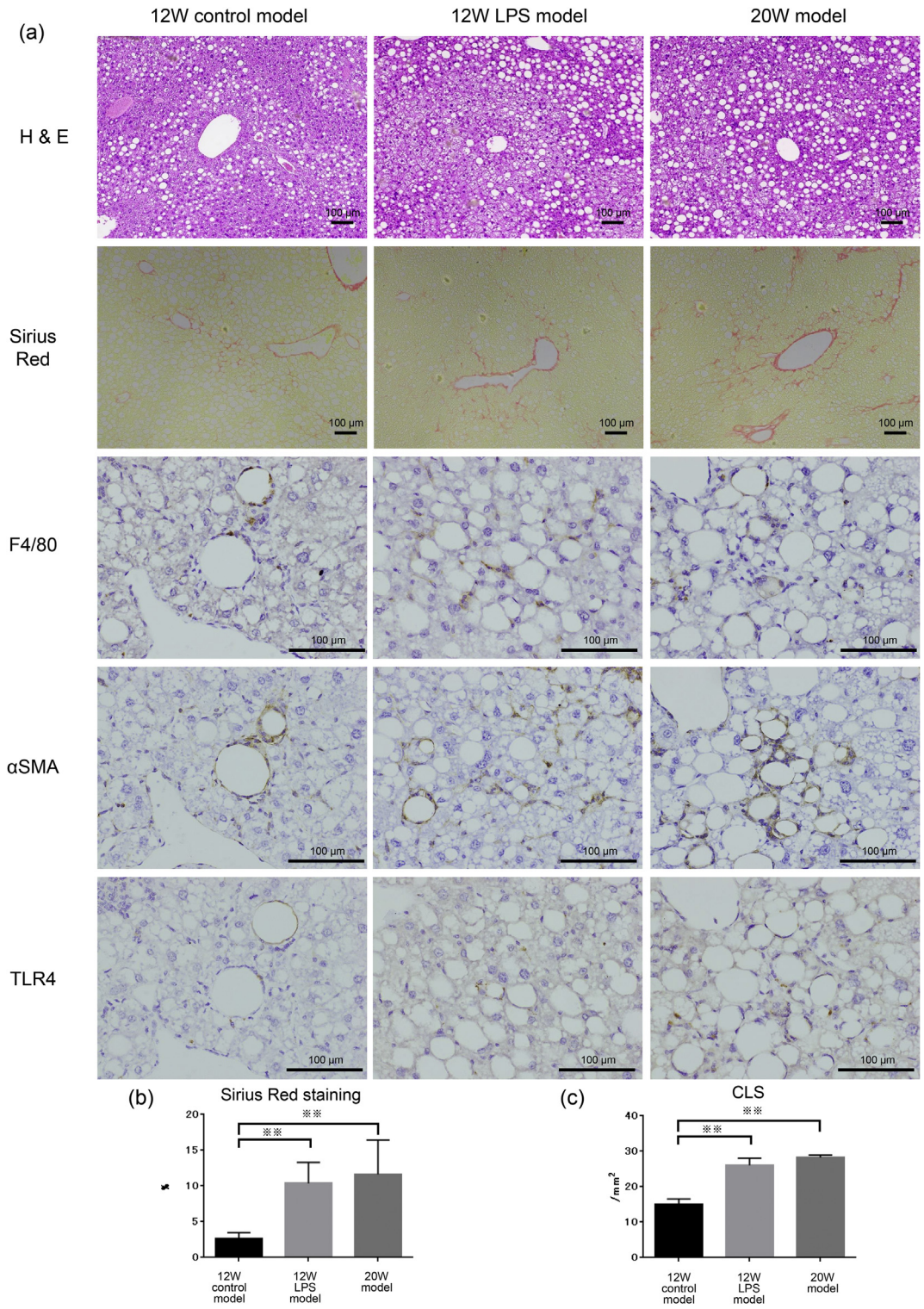

Fig. 3. Analysis of the effect of LPS. (a) H & E staining, (b) Sirius Red staining, and (c) immunohistochemistry for F4/80 are shown. (b) Quantitation of Sirius Red staining area and (c) calculation of F4/80-positive crown-like structures (CLS) were performed in the 12W control model (n = 8), 12W LPS model (n = 8), and 20W control model (n = 8) (※*$p < 0.05$, ※※ $p < 0.01$, one-way ANOVA, Bonferroni test). Scale bar, 100 μm.

the pancreas) intra-peritoneally at day 2 post-natal, and at 28 days of age, the mice were continuously fed a high-fat diet (HFD), resulting in the development of NASH [19]. In this study, we used *Mc4r*-KO mice, which developed obesity, insulin resistance, and liver steatosis and fibrosis; nonetheless, the time required for NASH development was still long. Hence, we used LPS to establish a model of rapid NASH development.

Schwimmer et al. studied the association of intestinal microbiota and NAFLD in children with obesity with and without NAFLD. They observed that lower α-diversity of the intestinal microbiome

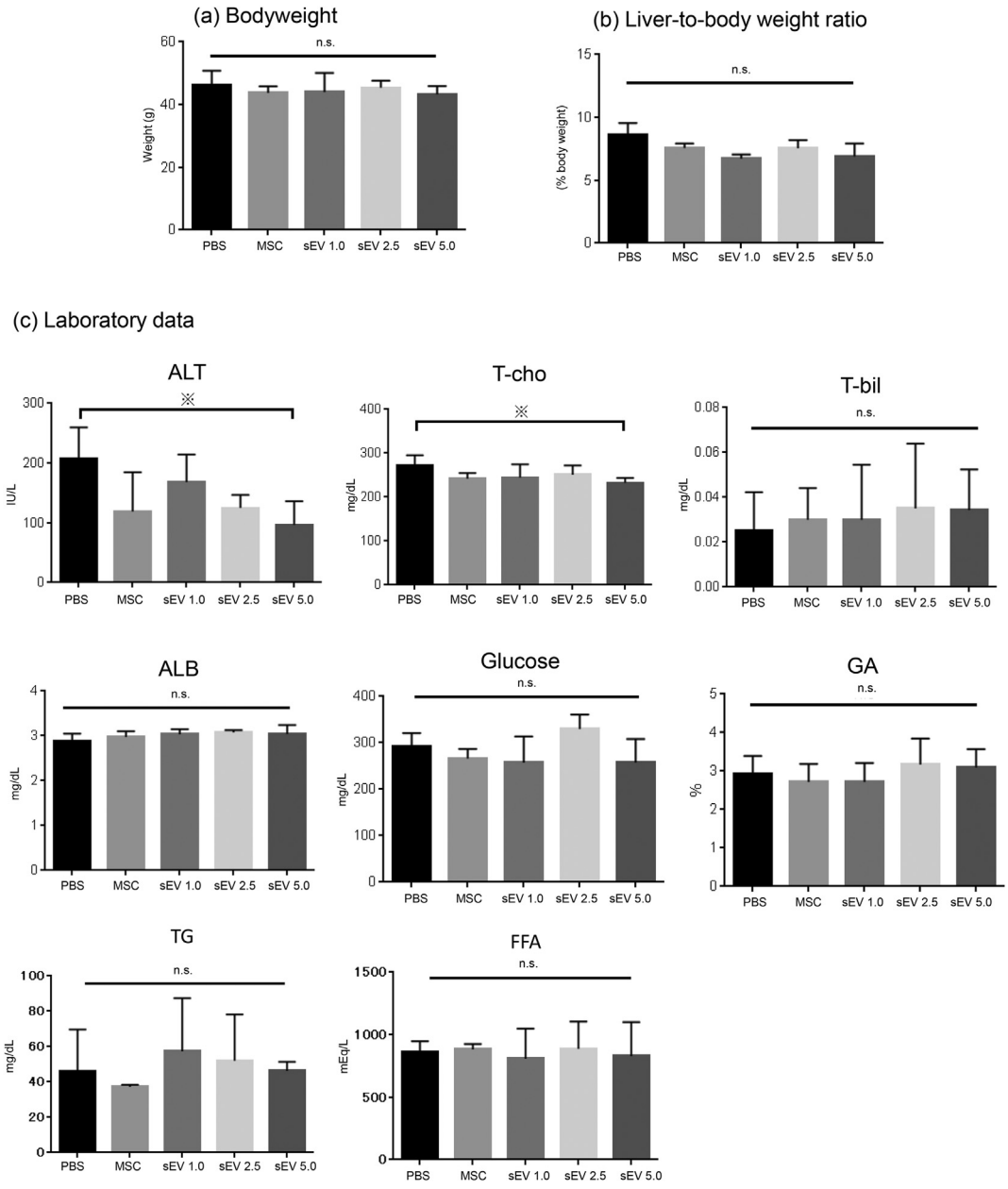

Fig. 4. Analysis of the therapeutic effect of MSCs and sEVs using a rapid fibrosis mouse model. (a) Bodyweight and (b) liver-to-body weight ratios were analyzed in each therapy group (n = 8). (c) Serum ALT, T-cho, T-bil, ALB, glucose, GA, TG, and FFA levels were also determined in each therapy group (n = 8) (※p < 0.05, ※※ p < 0.01, one-way ANOVA, Bonferroni test). ALT, alanine transaminase; T-cho, total cholesterol; T-bil, total bilirubin; ALB, albumin; GA, glycoalbumin; TG, triglyceride; FFA, free fatty acid.

was associated with both the presence and severity of NAFLD. They also reported that genes for LPS biosynthesis were upregulated under NASH conditions [20]. Song et al. reported that LPS treatment induces the accumulation of Yes-associated protein (YAP) in Kupffer cells both *in vitro* and in mice, which was prevented by macrophage/monocyte deletion of *Tlr4*. LPS transcriptionally activates YAP via AP-1 in macrophages/Kupffer cells. The LPS-induced YAP further enhances the expression of pro-inflammatory cytokines MCP-1, TNF-α, and IL-6 via association of YAP with the TEAD-binding motif in the promoter region of inflammatory cytokines [21]. Based on these observations, we speculated that *Mc4r*-KO mice treated with a WD and LPS could develop the pathological conditions of NASH faster than WD-treated *Mc4r*-KO mice. We believe that addition of LPS acts as "one of the hits" in the multiple-parallel hit hypothesis.

Currently, there are no approved drugs for the treatment of NASH, and diet therapy and exercise therapy are considered important for obtaining favorable outcomes [2]. In this context, MSCs and their sEVs are considered candidates for the treatment of NASH. Although the underlying mechanisms are still not fully understood, MSCs and sEVs exhibited anti-inflammatory and anti-fibrotic effects. Both therapies reduced ALT levels; in particular, sEV therapy reduced ALT levels in a dose-dependent manner. Furthermore, both MSC and sEV therapy decreased the number of CLS and the fibrosis area. Both MSCs and sEVs are reported to possess anti-inflammatory effects; for example, they can reduce T-cell activation and induce regulatory T cells and anti-inflammatory macrophages [10,22]. These effects may prevent the activation of hepatic stellate cells, thereby reducing fibrogenesis. Macrophages are possibly the target cells of MSCs and sEVs. Macrophages, which

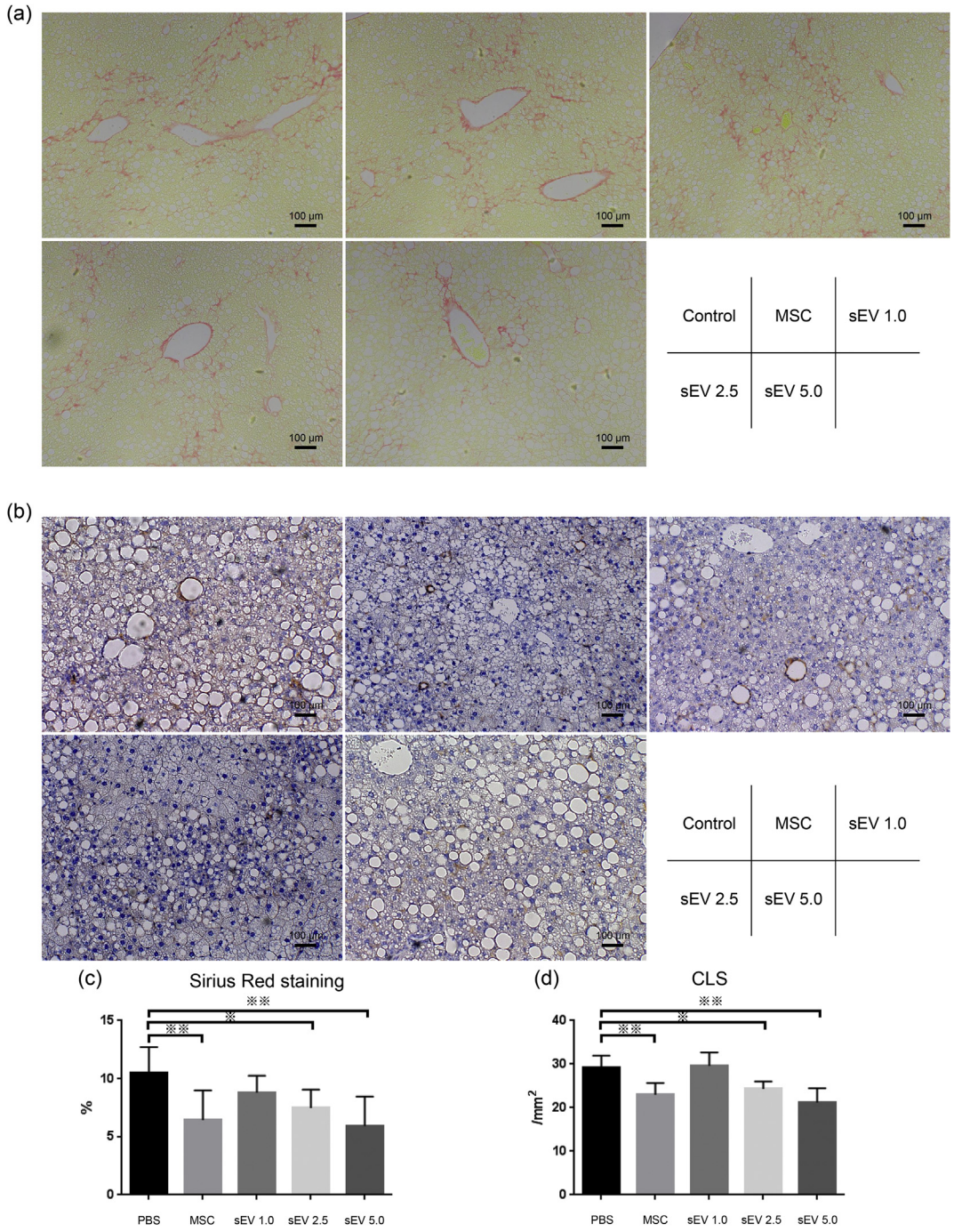

Fig. 5. Analysis of the fibrosis area and crown-like structures (CLS) after MSC and sEV therapy using the rapid fibrosis mouse model (a and c) Quantitation of the Sirius Red-stained area and (b and d) the F4/80-positive CLS were performed in each MSC and sEV therapy group (n = 8 per group) (※ $p < 0.05$, ※※ $p < 0.01$, one-way ANOVA, Bonferroni test). Scale bar, 100 μm.

possess both pro- and anti-inflammatory effects, are recruited to the damaged area, where they phagocytose the debris of hepatocytes. Previously, we have shown that MSC and bone marrow-derived macrophage (BMM) combination therapy is more effective in ameliorating fibrosis than MSC and BMM monotherapy [10]. In our current study, MSCs and sEVs induced anti-inflammatory macrophages. Considering our current and previous study, we suspect that induced anti-inflammatory macrophages may be related to MMP production and induce oncostatin M (OSM), for example, after phagocytosing hepatocyte debris. This induction of anti-inflammatory macrophages may be related to fibrolysis and promotion of regeneration [10]. Recently, Moroni et al. reported a first-in-human phase I dose-escalation study and analyzed the safety profile of autologous macrophage therapy. They collected CD14+ cells via leukapheresis and CiniMACS and cultured these with macrophage colony-stimulating factor (M-CSF) for 7 days. This study showed the importance of induction of appropriate macrophage polarization. *In vivo*, MSCs and sEVs can modulate the polarity of macrophages [23]. However, further analyses are necessary to elucidate the relationship between MSCs and macrophages.

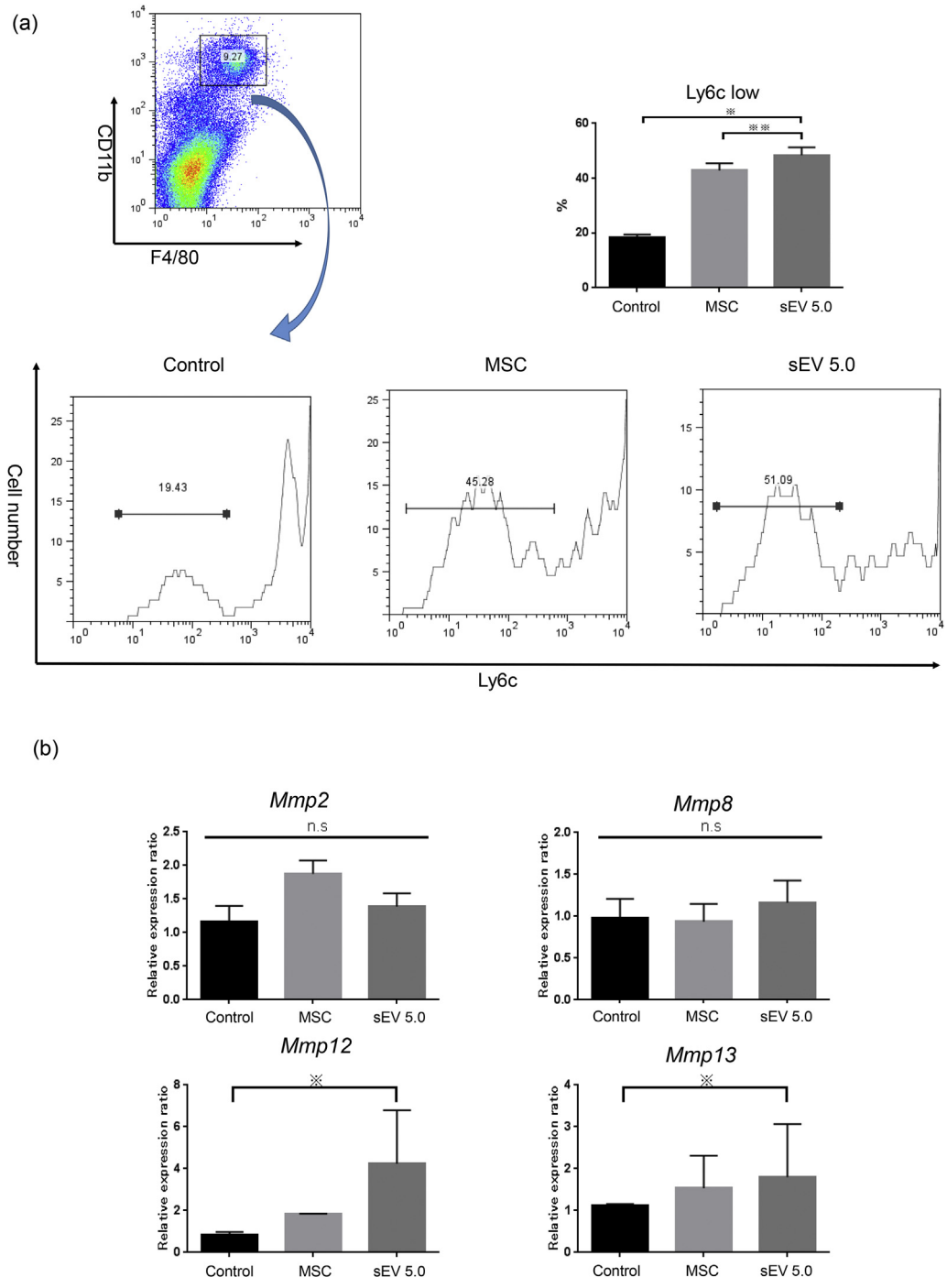

Fig. 6. Flow cytometric analysis of macrophages in the liver and qRT-PCR analysis of the liver tissue after treatment. (a) The frequency of Ly-6c^{low} cells among CD11b + F4/80+ cells was calculated in the PBS group (n = 5), MSC injection group (n = 5), and sEV injection group (5.0 μg/mouse; exo5.0; n = 5). (b) The changes in the mRNA expression of *Mmp2*, *Mmp8*, *Mmp12*, and *Mmp13* were analyzed in each group (n = 5 per group) (※ $p < 0.05$, ※※ $p < 0.01$, one-way ANOVA, Bonferroni test).

We observed that the therapeutic effects of MSCs and MSC-derived sEVs were similar for NASH, although the underlying mechanisms are not yet clear. Using two-photon excitation microscopy, we previously observed that most MSCs do not migrate into the liver; instead, most MSCs were trapped in the lung and disappeared from the lung, liver, and spleen in 7 days, suggesting that humoral factors, including the sEVs of MSCs, are important [10]. We suspect that owing to their small size, sEVs can be injected in large amounts without causing lung embolization. Indeed, some studies have reported that most sEVs are trapped in the liver for a short term after injection. Furthermore, no explicit immunogenicity has been reported in any cross-species studies on the use of sEVs [13,24]. Therefore, similar to their parent MSCs, sEVs from allogeneic MSCs are considered hypoimmunogenic. Thus, sEVs may be ideal treatment tools for liver diseases, including NASH. Currently, there are over 200 preclinical studies regarding sEV-based therapies in various animal models [13,24]. Thus, sEV therapy, which can induce anti-inflammatory and anti-fibrotic effects,

can be potentially used in various fields and can be developed commercially as a medical product.

One of the limitations of this study is that although the *Mc4r*-KO mouse is an ideal animal model for NASH, it does not completely represent the human situation and still requires a long time to mimic the conditions of human NASH. Furthermore, the contents of the sEVs have not yet been identified. Reports show that sEVs carry proteins, miRNAs, and lipids [25]; however, further studies are warranted to identify and characterize the specific components that possess therapeutic properties for NASH. Alternatively, the lipid bilayer-enclosed sEVs themselves may act as therapeutics owing to their stability, which also requires further investigation. Nonetheless, MSC-derived sEVs are attractive therapeutic tools for liver diseases, including NASH.

Author contributions

T.W. and A.T.: conception and design of the study; T.W., A.T., S.T., S.N., T.Y., M.O., and M.T.: generation, collection, analysis, and interpretation of data; T.W. and A.T.: writing of the manuscript; S.T.: supervision of the study.

Declaration of competing interest

The authors declare no conflict of interest.

Acknowledgments

This study was supported by a Grant-in-Aid for Scientific Research (B) (19H03636) from the Ministry of Education, Culture, Sports, Science, and Technology of Japan.

Appendix A. Supplementary data

Supplementary data to this article can be found online at https://doi.org/10.1016/j.reth.2020.03.012.

References

[1] Younossi ZM, Koenig AB, Abdelatif D, Fazel Y, Henry L, Wymer M. Global epidemiology of nonalcoholic fatty liver disease-Meta-analytic assessment of prevalence, incidence, and outcomes. Hepatology 2016;64:73–84.
[2] Yki-Jarvinen H. Non-alcoholic fatty liver disease as a cause and a consequence of metabolic syndrome. Lancet Diabetes Endocrinol 2014;2:901–10.
[3] Itoh M, Suganami T, Nakagawa N, Tanaka M, Yamamoto Y, Kamei Y, et al. Melanocortin 4 receptor-deficient mice as a novel mouse model of nonalcoholic steatohepatitis. Am J Pathol 2011;179:2454–63.
[4] Itoh M, Kato H, Suganami T, Konuma K, Marumoto Y, Terai S, et al. Hepatic crown-like structure: a unique histological feature in non-alcoholic steatohepatitis in mice and humans. PloS One 2013;8:e82163.
[5] Komiya C, Tanaka M, Tsuchiya K, Shimazu N, Mori K, Furuke S, et al. Antifibrotic effect of pirfenidone in a mouse model of human nonalcoholic steatohepatitis. Sci Rep 2017;7:44754.
[6] Shiba K, Tsuchiya K, Komiya C, Miyachi Y, Mori K, Shimazu N, et al. Canagliflozin, an SGLT2 inhibitor, attenuates the development of hepatocellular carcinoma in a mouse model of human NASH. Sci Rep 2018;8:2362.
[7] Itoh M, Suganami T, Kato H, Kanai S, Shirakawa I, Sakai T, et al. CD11c+ resident macrophages drive hepatocyte death-triggered liver fibrosis in a murine model of nonalcoholic steatohepatitis. JCI Insight 2017;2.
[8] Yamada T, Kashiwagi Y, Rokugawa T, Kato H, Konishi H, Hamada T, et al. Evaluation of hepatic function using dynamic contrast-enhanced magnetic resonance imaging in melanocortin 4 receptor-deficient mice as a model of nonalcoholic steatohepatitis. Magn Reson Imaging 2019;57:210–7.
[9] Tsuchiya A, Takeuchi S, Watanabe T, Yoshida T, Nojiri S, Ogawa M, et al. Mesenchymal stem cell therapies for liver cirrhosis: MSCs as "conducting cells" for improvement of liver fibrosis and regeneration. Inflamm Regen 2019;39:18.
[10] Watanabe Y, Tsuchiya A, Seino S, Kawata Y, Kojima Y, Ikarashi S, et al. Mesenchymal stem cells and induced bone marrow-derived macrophages synergistically improve liver fibrosis in mice. Stem Cells Transl Med 2019;8:271–84.
[11] Kojima Y, Tsuchiya A, Ogawa M, Nojiri S, Takeuchi S, Watanabe T, et al. Mesenchymal stem cells cultured under hypoxic conditions had a greater therapeutic effect on mice with liver cirrhosis compared to those cultured under normal oxygen conditions. Regen Ther 2019;11:269–81.
[12] Dominici M, Le Blanc K, Mueller I, Slaper-Cortenbach I, Marini F, Krause D, et al. Minimal criteria for defining multipotent mesenchymal stromal cells. The International Society for Cellular Therapy position statement. Cytotherapy 2006;8:315–7.
[13] Elahi FM, Farwell DG, Nolta JA, Anderson JD. Preclinical translation of exosomes derived from mesenchymal stem/stromal cells. Stem Cells 2020 Jan;38(1):15–21. https://doi.org/10.1002/stem.3061. Published online 2019 Oct 1.
[14] Reiner AT, Witwer KW, van Balkom BWM, de Beer J, Brodie C, Corteling RL, et al. Concise review: developing best-practice models for the therapeutic use of extracellular vesicles. Stem Cells Transl Med 2017;6:1730–9.
[15] Rohde E, Pachler K, Gimona M. Manufacturing and characterization of extracellular vesicles from umbilical cord-derived mesenchymal stromal cells for clinical testing. Cytotherapy 2019;21:581–92.
[16] Witwer KW, Van Balkom BWM, Bruno S, Choo A, Dominici M, Gimona M, et al. Defining mesenchymal stromal cell (MSC)-derived small extracellular vesicles for therapeutic applications. J Extracell Vesicles 2019;8:1609206.
[17] Balthasar N, Dalgaard LT, Lee CE, Yu J, Funahashi H, Williams T, et al. Divergence of melanocortin pathways in the control of food intake and energy expenditure. Cell 2005;123:493–505.
[18] Tsuchida T, Lee YA, Fujiwara N, Ybanez M, Allen B, Martins S, et al. A simple diet- and chemical-induced murine NASH model with rapid progression of steatohepatitis, fibrosis and liver cancer. J Hepatol 2018;69:385–95.
[19] Liebig M, Dannenberger D, Vollmar B, Abshagen K. n-3 PUFAs reduce tumor load and improve survival in a NASH-tumor mouse model. Ther Adv Chronic Dis 2019;10:2040622319872118.
[20] Schwimmer JB, Johnson JS, Angeles JE, Behling C, Belt PH, Borecki I, et al. Microbiome signatures associated with steatohepatitis and moderate to severe fibrosis in children with nonalcoholic fatty liver disease. Gastroenterology 2019;157:1109–22.
[21] Wang J, Song T, Zhou S, Kong X. YAP promotes the malignancy of endometrial cancer cells via regulation of IL-6 and IL-11. Mol Med 2019;25:32.
[22] Kawata Y, Tsuchiya A, Seino S, Watanabe Y, Kojima Y, Ikarashi S, et al. Early injection of human adipose tissue-derived mesenchymal stem cell after inflammation ameliorates dextran sulfate sodium-induced colitis in mice through the induction of M2 macrophages and regulatory T cells. Cell Tissue Res 2019;376:257–71.
[23] Moroni F, Dwyer BJ, Graham C, Pass C, Bailey L, Ritchie L, et al. Safety profile of autologous macrophage therapy for liver cirrhosis. Nat Med 2019;25:1560–5.
[24] Allan DS, Tieu A, Lalu M, Burger D. Concise review: mesenchymal stromal cell-derived extracellular vesicles for regenerative therapy and immune modulation: progress and challenges toward clinical application. Stem Cells Transl Med 2020 Jan;9(1):39–46. https://doi.org/10.1002/sctm.19-0114. Published online 2019 Aug 14.
[25] Kalluri R, LeBleu VS. The biology, function, and biomedical applications of exosomes. Science 2020;367.